Microwave-heating-coupled photoacoustic radar for tissue diagnostic imaging

Wei Wang
Andreas Mandelis

Microwave-heating-coupled photoacoustic radar for tissue diagnostic imaging

Wei Wang and Andreas Mandelis*
University of Toronto, Center for Advanced Diffusion Wave and Photoacoustic Technologies, Department of Mechanical and Industrial
Engineering, 5 King's College Road, Toronto M5S3G8, Canada

Abstract. An investigation of microwave (MW) heating effects on biotissue for enhancing photoacoustic radar (PAR) signals was conducted. Localized tissue heating generated by MWs was used to improve PAR imaging depth and signal-to-noise ratio (SNR). Elevated temperatures were measured with thermocouples in *ex vivo* bovine muscle. The measured temperature rise on the heated spot surface by MWs was in agreement with theoretical predictions. The study showed localized MW heating can increase the photoacoustic imaging depth by 11%, and the SNR by 5% in *ex vivo* bovine muscle. © *2016 Society of Photo-Optical Instrumentation Engineers (SPIE)* [DOI: 10.1117/1.JBO.21.6.066018]

Keywords: photoacoustic imaging; microwave heating; photoacoustic radar; temperature.

Paper 150488RRR received Jul. 20, 2015; accepted for publication Jun. 13, 2016; published online Jun. 29, 2016.

1 Introduction

Photoacoustic (PA) imaging combines the advantages of high contrast of light absorption, high resolution, and penetration depth of ultrasound, and has been investigated for breast cancer detection in recent years.[1,2] The performance characteristics of PA imaging systems include the maximum imaging depth, sensitivity, resolution, and contrast.[3,4] PA imaging has good sensitivity, resolution, and contrast, but the major limitation is the optical penetration depth.[3–5] Light intensity decreases exponentially with penetration depth because of strong scattering and absorption in biological tissues.[6,7] The optical window in the range of 700 to 900 nm allows relatively higher light penetration depth.[6,7] PA signals can be improved by contrast agents, such as silica-coated super paramagnetic iron oxide nanoparticles,[8] system optimization, signal processing, or higher laser power.[9] However, contrast agents have side effects, system optimization increases the complexity and cost, and higher laser power exposure induces potential damage to skin.

Manipulation of tissue temperature has been used for thermal ablation, hyperthermia, and imaging.[10–13] The normal body temperature of a healthy adult is ∼37°C.[14,15] Studies show that most normal healthy tissues such as liver, kidney, and muscles can withstand temperatures up to 44°C for 30 min.[10,16–18] The relationship between thermal exposure time and temperature in most normal healthy tissues has also been studied.[18,19] The reported results show that heating effects of 60-min exposure time at 43°C are equivalent to 30 (15) min of exposure at 44°C (45°C). These and other results indicate that there exist ranges of maximum safe exposure times at substantially higher temperatures than normal for most normal healthy tissues,[16,17,20] and thus the possibility of using high temperature for significant improvements in the PA signal strength and imaging depth. Thermal energy can be locally delivered by microwaves (MWs) in biological tissues.[11] An MW-energy applicator (antenna) is placed on the target site to increase the temperature surrounding the applicator inside the tissue. Coaxial slot antennas are the most popular tools for MW heating purposes due to their small dimensions and low cost.[21,22]

Generally speaking, two kinds of laser sources are used to generate PA signals: (1) pulsed and (2) continuous wave (CW)-modulated laser sources. The pulsed laser is the conventional laser source, but CW lasers have the advantages of low cost, portability, and narrow band detection [i.e., high signal-to-noise ratio (SNR)].[9] The photoacoustic radar (PAR) uses chirp signals for laser-beam modulation and matched filtering for signal processing.[23] Temperature can affect PAR signals, which become stronger at higher temperatures.[12,13] The imaging depth and SNR can be improved through uniform heating.[12,13] Most research reports of MW heating have been in applications of surgical ablation.[21,22,24–27] Our earlier study[12] showed that "under uniform heating," the thermally enhanced PA radar probe can increase the signal strength from *ex vivo* beef muscle by 13% and the imaging depth over 20% with a temperature increase from 37°C to 43°C. However, imaging improvement through uniform heating takes very long and can cause discomfort and inconvenience to patients. Thus, it is necessary to find a localized heating method for precise tissue targeting and shortening the exposure time. The present feasibility study investigates the thermal effects on PAR signal enhancement "under targeted (localized)" heating of biotissues in the same temperature range using MW heating. The tradeoff was found to be rapid (localized MW) heating at relatively low signal strength increase versus very slow uniform heating with significantly higher signal strength increase.

2 Theoretical Background

PAR signals were generated by harmonically modulating light illumination on absorbers.[28] The response amplitude spectrum $\tilde{p}(\omega)$ of the generated acoustic pressure can be written in one dimension as[12,23,29]

$$|\tilde{p}(\omega)| = \frac{\mu_a \Gamma e^{-\mu_{ef} z}}{\sqrt{\mu_a^2 c_a^2 + \omega^2}} E_0, \tag{1}$$

*Address all correspondence to: Andreas Mandelis, E-mail: mandelis@mie.utoronto.ca

where μ_a represents the optical absorption coefficient (m^{-1}), ω is the angular modulation frequency (rad/s), Γ is the Grüneisen parameter (dimensionless), μ_{ef} is the effective optical attenuation coefficient (m^{-1}), c_a is the speed of sound (m/s), z is the subsurface distance (m), and E_0 is the optical fluence at the surface of the absorber (J $\cdot$ Hz/m^2). The Grüneisen parameter is defined as

$$\Gamma = \frac{\beta c_a^2}{c_p}, \tag{2}$$

where c_p is the specific heat capacity [J/(kg $\cdot$ °C)]. The matched-filter pulse compression method was introduced into the PAR system to give the frequency-domain PA signal necessary depth resolution and adequate SNR.[28] Matched filtering is introduced by the cross-correlation method to measure the similarity of two signals (frequency content and phase). The cross-correlation output is

$$R(t) = \int_{-\infty}^{+\infty} r(\tau - t) \cdot s(\tau) d\tau, \tag{3}$$

where $s(t)$ and $r(t)$ are the detected and reference signals, respectively. Linear frequency modulation (LFM) is the simplest and most popular signal pulse compression method, which can reduce side lobes and improve depth resolution, among other attributes.[28,30] An LFM signal can be expressed as

$$r_t = \mathrm{rect}\left(\frac{t}{2K}\right) \cos\left(\omega_0 t + \frac{\pi B}{K} t^2\right), \quad -\frac{K}{2} \le t \le \frac{K}{2}, \tag{4}$$

where ω_0 is the center angular frequency, K is the pulse duration, and B is the frequency bandwidth. The output of a matched filter can be written as

$$R_t = \frac{K}{2} \mathrm{rect}\left(\frac{t}{2K}\right) \frac{\sin\left[\pi B t\left(1 - \frac{t}{K}\right)\right]}{\pi B t} \cos(\omega_0 t). \tag{5}$$

In frequency-domain signal processing, the Fourier transform of the reference signal r_t is $\tilde{r}(\omega)$ and the complex conjugate of $\tilde{r}(\omega)$ is $\tilde{h}(\omega)$. The matched filter output $\tilde{R}(\omega)$ in the frequency domain is obtained as

$$\tilde{R}(\omega) = \tilde{s}(\omega) \cdot \tilde{h}(\omega). \tag{6}$$

The spectrum of the LFM signal r_t is

$$\tilde{r}(\omega) = \frac{1}{2} \int_{-\frac{K}{2}}^{\frac{K}{2}} e^{j\left[(\omega_0 - \omega)t + \frac{\pi B}{K} t^2\right]} dt + \frac{1}{2} \int_{-\frac{K}{2}}^{\frac{K}{2}} e^{-j\left[(\omega_0 - \omega)t + \frac{\pi B}{K} t^2\right]} dt. \tag{7}$$

The Fresnel integrals $C(X)$ and $S(X)$ are defined by

$$C(X) = \int_0^X \cos \frac{\pi y^2}{2} dy, \tag{8}$$

$$S(X) = \int_0^X \sin \frac{\pi y^2}{2} dy. \tag{9}$$

It can be shown that

$$\tilde{r}(\omega) = \frac{1}{2}\sqrt{\frac{K}{2B}}\left\{ e^{\frac{-j(\omega-\omega_0)^2}{4\pi B}}[C(x_3) + C(x_4) + jS(x_3) + jS(x_4)] \right\}$$
$$+ \frac{1}{2}\sqrt{\frac{K}{2B}}\left\{ e^{\frac{j(\omega+\omega_0)^2}{4\pi B}}[C(x_5) + C(x_6) - jS(x_5) - jS(x_6)] \right\}, \tag{10}$$

where

$$x_3 = \sqrt{\frac{\Omega}{\pi}}\left(\frac{K}{2} + \frac{\omega - \omega_0}{\Omega}\right), \tag{11}$$

$$x_4 = \sqrt{\frac{\Omega}{\pi}}\left(\frac{K}{2} - \frac{\omega - \omega_0}{\Omega}\right), \tag{12}$$

$$x_5 = \sqrt{\frac{\Omega}{\pi}}\left(\frac{K}{2} + \frac{\omega + \omega_0}{\Omega}\right), \tag{13}$$

$$x_6 = \sqrt{\frac{\Omega}{\pi}}\left(\frac{K}{2} - \frac{\omega + \omega_0}{\Omega}\right), \tag{14}$$

where $\Omega = (2\pi B / K)$. Thus, the complex conjugate of $\tilde{r}(\omega)$ is given as

$$\tilde{h}(\omega) = \frac{1}{2}\sqrt{\frac{K}{2B}}\left\{ \cos \frac{(\omega-\omega_0)^2}{4\pi B}[C(x_3) + C(x_4)] + \cos \frac{(\omega+\omega_0)^2}{4\pi B}[C(x_5) + C(x_6)] \atop + \sin \frac{(\omega-\omega_0)^2}{4\pi B}[S(x_3) + S(x_4)] + \sin \frac{(\omega+\omega_0)^2}{4\pi B}[S(x_5) + S(x_6)] \right\}$$
$$+ \frac{j}{2}\sqrt{\frac{K}{2B}}\left\{ \sin \frac{(\omega-\omega_0)^2}{4\pi B}[C(x_3) + C(x_4)] - \sin \frac{(\omega+\omega_0)^2}{4\pi B}[C(x_5) + C(x_6)] \atop - \cos \frac{(\omega-\omega_0)^2}{4\pi B}[S(x_3) + S(x_4)] + \cos \frac{(\omega+\omega_0)^2}{4\pi B}[S(x_5) + S(x_6)] \right\}. \tag{15}$$

The amplitude of $\tilde{h}(\omega)$ and $\tilde{s}(\omega)$ can be derived as

$$|\tilde{h}(\omega)| = |\tilde{s}(\omega)|$$
$$\approx \frac{1}{2}\sqrt{\frac{K}{2B}}\sqrt{\frac{[C(x_3) + C(x_4)]^2 + [C(x_5) + C(x_6)]^2}{+ [S(x_3) + S(x_4)]^2 + [S(x_5) + S(x_6)]^2}}. \tag{16}$$

Fresnel integrals can be approximated as[31]

$$C(x) \approx \frac{1}{2} + \frac{1}{\pi x} \sin\left(\frac{\pi x^2}{2}\right), \quad \text{for } x \gg 1, \tag{17}$$

$$S(x) \approx \frac{1}{2} - \frac{1}{\pi x} \cos\left(\frac{\pi x^2}{2}\right), \quad \text{for } x \gg 1. \tag{18}$$

For frequencies higher than 300 kHz, the Fresnel integrals are ~1/2. Therefore, the final matched filter output amplitude spectrum of two signals $\tilde{h}(\omega)$ and $\tilde{s}(\omega)$ is approximately[32] given by

$$|\tilde{s}(\omega) \cdot \tilde{h}(\omega)| \approx \frac{K}{2B}. \tag{19}$$

The output amplitude spectrum is proportional to the duration of the chirp and inversely proportional to the bandwidth of the chirp. For narrow frequency bandwidth B and long duration time K chirps, the amplitude increases.

Water plays an important role in biotissues. The total water content of human tissues can be up to 77%.[33] The Grüneisen parameter of water increases monotonically from 0.11 at 20°C to 0.24 at 45°C [shown in Fig. 1(a)]. The thermal expansion coefficient increases 107% from 20°C to 45°C.[34] The specific heat capacity of water is a mildly temperature-dependent parameter and the variation is less than 1% from 20°C to 45°C.[35] The speed of sound in water increases with temperature from 1482 to 1536 m/s, which is 3.6% increase from 20°C to 45°C.[36] Figure 1(b) shows a comparison of the temperature dependence of the parameters constituting the Grüneisen constant. It can be seen that the thermal expansion coefficient contributes much more than the other two parameters to the increase.

Bovine muscles are used as samples for experimental validation. Myoglobin and hemoglobin are the main light absorbers in bovine muscle tissues and the concentration of myoglobin is much higher than hemoglobin:[37] Myoglobin content is 0.41 mmol/kg, whereas hemoglobin content is only 0.066 mmol/kg in bovine muscle.[37] Myoglobin concentration can determine the color of muscle: higher myoglobin concentration yields darker color.[38] In *ex vivo* tissues, myoglobin and hemoglobin are present in oxygenated or deoxygenated forms, but deoxygenated concentrations are higher. On the surface of *ex vivo* tissues, the degree of oxygenated concentrations is higher. After myoglobin is oxygenated (oxymyoglobin), color changes from dark purple to bright red, with the muscle assuming a bright cherry-red color.[38]

A typical composition of bovine muscle consists approximately of 75% water, 19% protein, 3% fat, 1% fiber, 1% carbohydrate, and 1% ash.[39,40] Temperature-dependent empirical thermal property models of individual biotissue-components have been introduced for the Grüneisen parameter estimation.[12,41] The Grüneisen parameter of a typical bovine

muscle dependence on temperature has been studied from 20°C to 45°C.[12] In this temperature range, the increase is 67% for the Grüneisen parameter, 1.2% for the speed of sound, 0.33% for the specific heat capacity, and 64% for the thermal expansion coefficient.[12] The highest increase is, again, the thermal expansion coefficient.

The PAR signal changes with the Grüneisen parameter, and thus becomes temperature dependent.[42–44] Temperature rise in tissue depends on both heating power and time, and is also related to tissue properties and heat transfer to the vasculature.[12] The specific absorption rate (SAR) describes the time-averaged amount of MW power deposited per unit mass of tissue (W/kg). The SAR of electromagnetic energy incident on a tissue sample is defined by

$$SAR = \frac{\sigma}{2\rho} |E|^2, \tag{20}$$

where σ is the electrical conductivity of biological tissue (S/m), ρ is its density (kg/m^3), and $|E|$ is the amplitude of the applied electric field (V/m). The SAR determines the heating pattern of the MW applicator (antenna) in tissue. Its depth distribution can be approximately expressed as an exponential profile[45]

$$SAR = S_0 e^{-\mu' z}, \tag{21}$$

where S_0 represents the amplitude of SAR at the surface, z is the distance from the heated spot (m), and μ' represents the MW energy absorption coefficient (m^{-1}).

The MW-generated heat is strongly dependent on the absorption coefficient of tissue, and on the frequency and intensity of the energy source.[46] Heat can be reduced by increasing perfusion with temperature.[47] Assuming that tissue is electromagnetically heterogeneous and acoustically homogeneous, the Pennes bioheat transfer equation was developed for roughly describing temperature elevation in biological tissues[47]

$$\rho c_p \frac{\partial T}{\partial t} = k\nabla^2 T - \rho_b c_b w_b (T - T_b) + q, \tag{22}$$

where T is the tissue temperature (°C), c_p is the tissue specific heat capacity [J/(kg · °C)], ρ is the tissue density, k is the tissue thermal conductivity [W/(m · °C)], w_b is the blood flow rate through the tissue [m^3/(s · kg)], ρ_b is the blood density, c_b is the blood specific heat capacity, T_b is the blood temperature
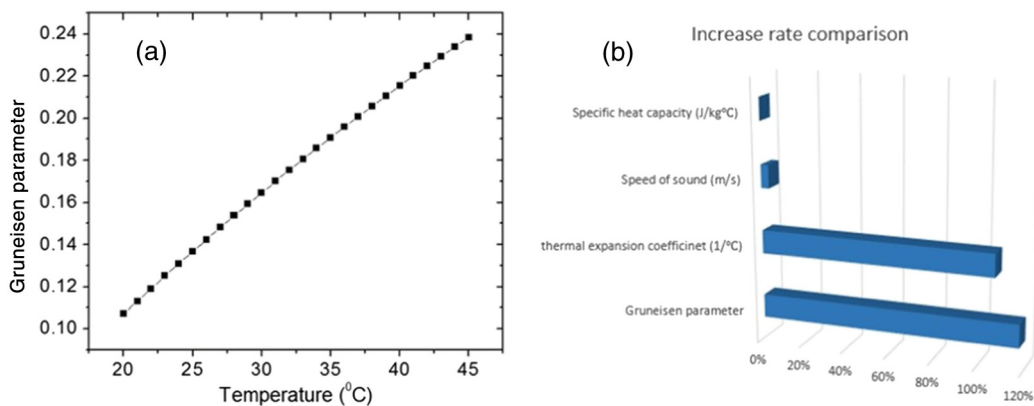

Fig. 1 (a) Grüneisen parameter of water dependence on temperature and (b) increase rate comparison of Grüneisen parameter elements of water from 20°C to 45°C.

(°C), t is the heating time (s), and q is the volume heating source (W/m^3). All temperature information about blood perfusion is included in the term $\rho_b w_b c_b (T - T_b)$. For *ex vivo* experiments, the blood perfusion term $w_b c_b = 0$. Due to the efficiency of MW heating, the heating time is less than half a minute. So for *in vivo* study, the blood flow effects can be ignored in such short time for tissues having low blood flow velocity, such as skeletal muscles. Thus, Eq. (22) can be simplified as[48]

$$\rho c_p \frac{\partial T}{\partial t} = k \nabla^2 T + q. \tag{23}$$

For MW heating, the geometry is shown in Fig. 2(a), where the cylindrical coordinate system is used. (r, z, t), (r', z', τ) are the observation and source coordinates, respectively. The translated temperature of the thermal field in the medium is written as

$$\theta(r, z, t) \equiv T(r, z, t) - T_0, \tag{24}$$

where T_0 is the ambient temperature. The translated thermal field satisfies the following equation:

$$\rho c_p \frac{\partial \theta}{\partial t} = \frac{k}{r} \frac{\partial}{\partial r} \left(r \frac{\partial \theta}{\partial r} \right) + k \frac{\partial^2 \theta}{\partial z^2} + q(r, z). \tag{25}$$

The initial and boundary conditions for MW heating are given by

$$\theta(r, z, 0) = 0, \tag{26}$$

$$\frac{\partial \theta(r, 0, t)}{\partial z} = 0, \tag{27}$$

$$q(z') = q_0 e^{-\mu' z'}, \tag{28}$$

$$q_0 = \eta \cdot \rho \cdot S_0, \tag{29}$$

where q_0 is the heat flux at the surface $z = 0$ and η is the heat generation efficiency. Here q is the MW source power, taken to be only a function of the depth (axial) coordinate and assumed uniform along the radial dimension, consistent with our experiments. The solution of the boundary value problem Eqs. (25) to (29) can be derived using the Green function (GF) method

$$\theta(r, z, t) =$$
$$\frac{1}{\rho c_p} \int_{\tau=0}^{t} \int_{r'=0}^{b} \int_{z'=0}^{L} q(z') G(r, z, t | r', z', \tau) 2\pi r' \, d\tau \, dr' \, dz'. \tag{30}$$

For the geometry shown in Fig. 2(a), it is assumed that the absorbing medium is cylindrical and semi-infinite lengthwise, $0 < r' < b$ in the radial direction, and the penetration depth is $L = 1/\mu'$ in the axial direction, corresponding to the absorbing area of the MW energy. The GF is separated into the product of a radial and an axial function[49]

$$G(r, z, t | r', z', \tau) = G_R(r, t | r', \tau) G_A(z, t | z', \tau). \tag{31}$$

The radial function G_R satisfies

$$G_R(r, t | b, 0) = G_R(r, t | 0, \tau) = 0, \tag{32}$$

where G_R is given by[50]

$$G_R(r, t | r', \tau) = \frac{1}{4\pi\alpha(t - \tau)} \exp\left[-\frac{(r^2 + r'^2)}{4\alpha(t - \tau)} \right]$$
$$\times I_0 \left[\frac{rr'}{2\alpha(t - \tau)} \right], \tag{33}$$

where I_0 is the modified Bessel function of the first kind of order zero and α is the thermal diffusivity $(\alpha = (k/\rho c_p))$. The axial function satisfies the following condition:

$$\frac{\partial}{\partial z'} G_A(z, t | z', \tau)|_{z'=0} = 0, \tag{34}$$

and is given by[50]

$$G_A(z, t | z', \tau) = \frac{1}{\sqrt{4\pi\alpha(t - \tau)}} \left\{ \exp\left[-\frac{(z - z')^2}{4\alpha(t - \tau)} \right] \right.$$
$$\left. + \exp\left[-\frac{(z + z')^2}{4\alpha(t - \tau)} \right] \right\}. \tag{35}$$
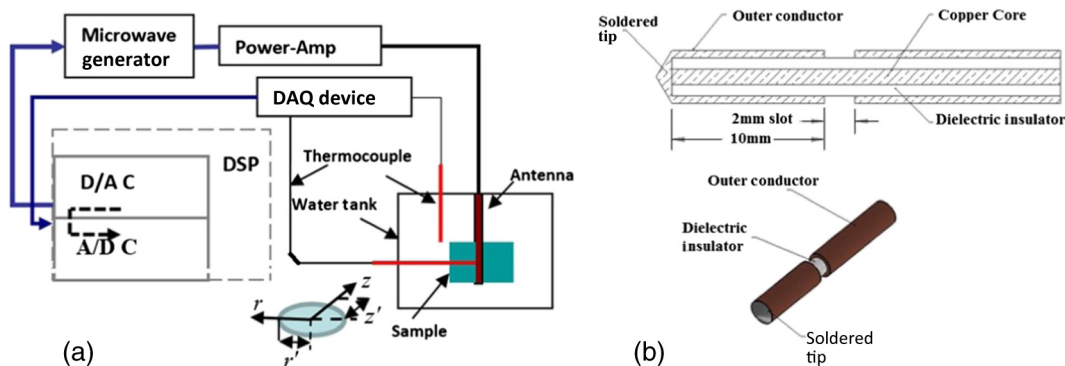
Thus, the solution of Eq. (30) is

Fig. 2 (a) Experimental setup for MW heating and (b) geometry of MW antenna.

$$\theta(r, z, t) = \frac{1}{\rho c_p} \int_{\tau=0}^{t} d\tau \int_{r'=0}^{b} G_R(r, t|r', \tau) 2\pi r' dr'$$

$$\times \int_{z'=0}^{L} q(z') G_A(z, t|z', \tau) dz'. \quad (36)$$

This yields

$$\theta(r, z, t) = \frac{q_0}{\rho c_p} \int_{\tau=0}^{t} d\tau \int_{r'=0}^{b} \frac{2\pi r'}{4\pi\alpha(t-\tau)} \exp\left[-\frac{(r^2 + r'^2)}{4\alpha(t-\tau)}\right]$$

$$\times I_0\left[\frac{rr'}{2\alpha(t-\tau)}\right] dr'$$

$$\times \int_{z'=0}^{L} \frac{1}{\sqrt{4\pi\alpha(t-\tau)}} \left\{ \exp\left[-\frac{\mu'z' + (z - z')^2}{4\alpha(t-\tau)}\right] \right.$$

$$\left. + \exp\left[-\frac{\mu'z' + (z + z')^2}{4\alpha(t-\tau)}\right] \right\} dz'. \quad (37)$$

For small values of b, at $r = 0$, $z = 0$, the solution is simplified as[50]

$$\theta(r, z, t)\bigg|_{\substack{r = 0 \\ z = 0}} = \frac{q_0}{k\sqrt{\pi}} (\alpha t)^{1/2}. \quad (38)$$

Tumors contain higher water content than normal healthy tissues,[51] and thus they have higher electrical conductivity than low-water-content healthy tissue.[52–54] Studies have shown that their electrical conductivity is about 10% higher than normal tissue.[55,56] This suggests that MWs can raise the temperature of tumor tissues higher than that of the host mammary tissues, and thus generate higher contrast between tumors and normal tissues. The MW penetration depth is the inverse of the microwave absorption coefficient, where the electric field power is reduced by $1/e^2$[46] at depths between 8.5 cm for bovine fat tissue and 1.1 cm for bovine muscle tissue at 2.45 GHz, respectively.[46,52,57] Penetration depths in other tissues have values between those of fat and muscle.

3 Experimental Setups

The experimental setup for MW heating used in this work consisted of a MW generator (SSG-4000HP, Mini-circuit), a 40-dB power amplifier (ZHL-16W-43+, Mini-circuit), a coaxial slot antenna, thermocouples, and a data-acquisition device (USB-6221, NI) as shown in Fig. 2(a). The generated MW signals were amplified with a power amplifier and then sent to the coaxial slot antenna. Since water is a good absorber of MW energy, an external waveguide applicator has difficulty in delivering the MW energy to the absorber immersed in the water (our setup), so a single-slot coaxial antenna was employed for this research. This type of antenna can locally produce an electromagnetic field around the slots and heat the target area (deep inside the absorber) efficiently.[21,22,24] The electrical power supplied to the antenna was set at 2 W. The frequency was set at 2.45 GHz, the most popular frequency used for hyperthermia and heating applications.[21,22,24] The coaxial slot antenna was constructed from a RG402 semirigid coaxial copper cable as shown in Fig. 2(b). The outer conductor and core were both made of copper. A 2-mm ring-shaped slot was cut by removing a part of the outer conductor near the tip of the cable. The outer and inner conductors were connected at the tip by soldering. The reflected signal was sampled at the reflected port of a directional coupler, and measured by a network analyzer (E5063A, Agilent). The measured power loss was about −12 dB (about 5% loss). Fine-wire thermocouples (K-type, Omega) were employed for temperature measurements. The measured data were collected by a USB DAQ device (USB-6221, NI), and then sent to a computer synchronized with the MW generator.

The experimental setup diagram for the MW-enhanced PAR system is shown in Fig. 3(a). A CW diode laser emitting at 800 nm was employed. The light beam size was 3.5 mm and was modulated by linear frequency waveform chirps (0.3 to 1.3 MHz, 1 ms in duration) generated by the signal-generation card NI PXI-5421 (National Instruments, Austin, Texas). A focused ultrasound transducer (Panametrics-NDT, V314) was utilized as a detector. The detected signals were amplified with a preamplifier (Panametrics-NDT, 5676) first, and then were sent to the digital data-acquisition card NI PXIe-5122 (National Instruments, Austin, Texas) in a computer. The sampling rate of the data-acquisition card NI PXIe-5122 was 100 MS/s, and the maximum input voltage was 10 V. Bovine muscle was purchased from a local store and was stored in a refrigerator at 4°C. Most experiments were performed within 3 days from the purchase. Fresh samples used for each experiment were cut from the same part. The sample
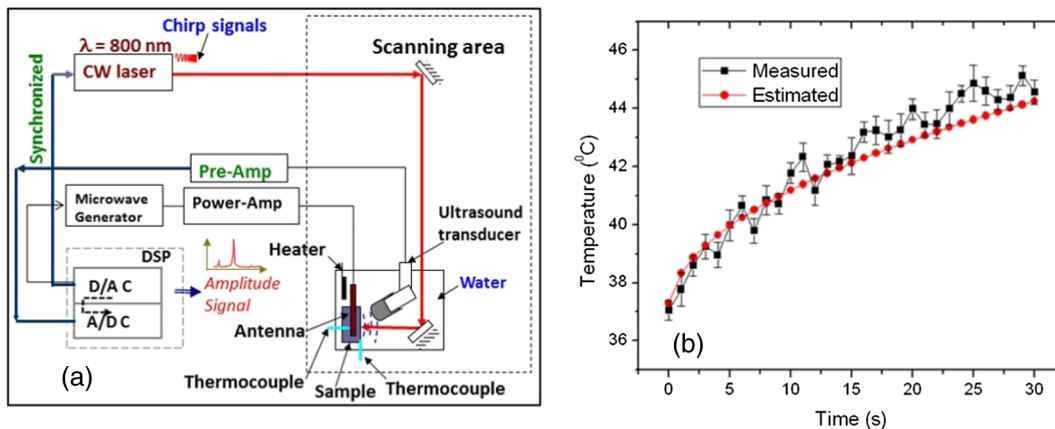

Fig. 3 (a) Experimental setup of the MW coupled PAR system and (b) measured temperature on a heated surface spot of bovine muscle versus time compared with the analytically estimated MW heating temperature.

dimensions were 30-mm long, 30-mm wide, and 20-mm thick. The samples were all wrapped in thin transparent plastic wrap during the experiments.

4 Results and Discussion

Figure 3(b) shows the comparison of the experimentally measured temperature in *ex vivo* bovine muscle of the MW-heated surface spots with the estimated temperature using Eq. (38). For bovine muscle at 37°C, the density is 1073.445 kg/m^3,[12,41] the specific heat capacity is 3632.7 J/(kg · °C),[12,41] and the thermal conductivity is 0.5228 W/(m · °C).[41,46] These parameters are all temperature dependent, but the variations are all less than 2% from 37°C to 45°C,[12,41] and are thus ignored in this study. The thermal diffusivity of bovine muscle can be calculated from the defining equation $\alpha = (k/\rho c_p)$. This yields $\alpha = 1.34 \times 10^{-7}$ m^2/s in the range 37°C to 45°C, so variation with T is ignored. For the 30-s heating period in Fig. 3(b), all the absorbed energy was assumed converted to heat ($\eta = 100\%$), and the experimentally measured temperature at the heated surface spot was in excellent agreement with the analytically estimated temperature. The SAR was estimated to be 3.1 W/kg (the best-fit value of the theory to the experimental results). The estimated error between measured and theoretical results was less than 10%. The temperature rose to 44.5°C from 37°C after 30-s of MW heating, a 20% increase. No visible damage was observed after the heating experiment.

Figure 4(a) shows the amplitude of the cross-correlation peak between the reference (by a uniform heating method) and the measured PAR signals under the influence of MW heating. The results showed that the PAR signal strength increased by about 8% with MW heating at ambient temperature 37°C and the SNR increased by 5%. The average elevated temperature during the PAR measurement was ~42°C. In comparison, with uniform heating, the PAR-signal-amplitude increased up to 13% from 37°C to 42°C with the sample immersed in heated water. For MW heating-assisted PAR, the nonuniformly distributed temperature field in tissue was generated by the MW applicator, and at lower temperatures, the PA signals were weaker.[12] Therefore, the nonuniform temperature distribution and the lower heating efficiency under MW heating were the reasons for the less-efficient PAR signal increase. Theoretically, the SNR can be improved by a further 8% with a more efficient thermally assisted method,[12,13] the single most important criterion for such efficiency being achieving temperature uniformity. The experimental results of the imaging depth enhancement study are shown in Fig. 4(b). The sample was placed in a box filled with 0.47% intralipid solution simulating an optical scatterer as shown in Fig. 4(c).[12,58] The estimated scattering coefficient of the 0.47% intralipid solution was 0.014 mL^{-1} L mm^{-1} (concentration × sample thickness) and the absorption coefficient was 0.003 mL^{-1} L mm^{-1}.[12,58] The box was translated with microstages to attain different subsurface absorber depths. At 18 mm, the PAR signal was measured with large errors
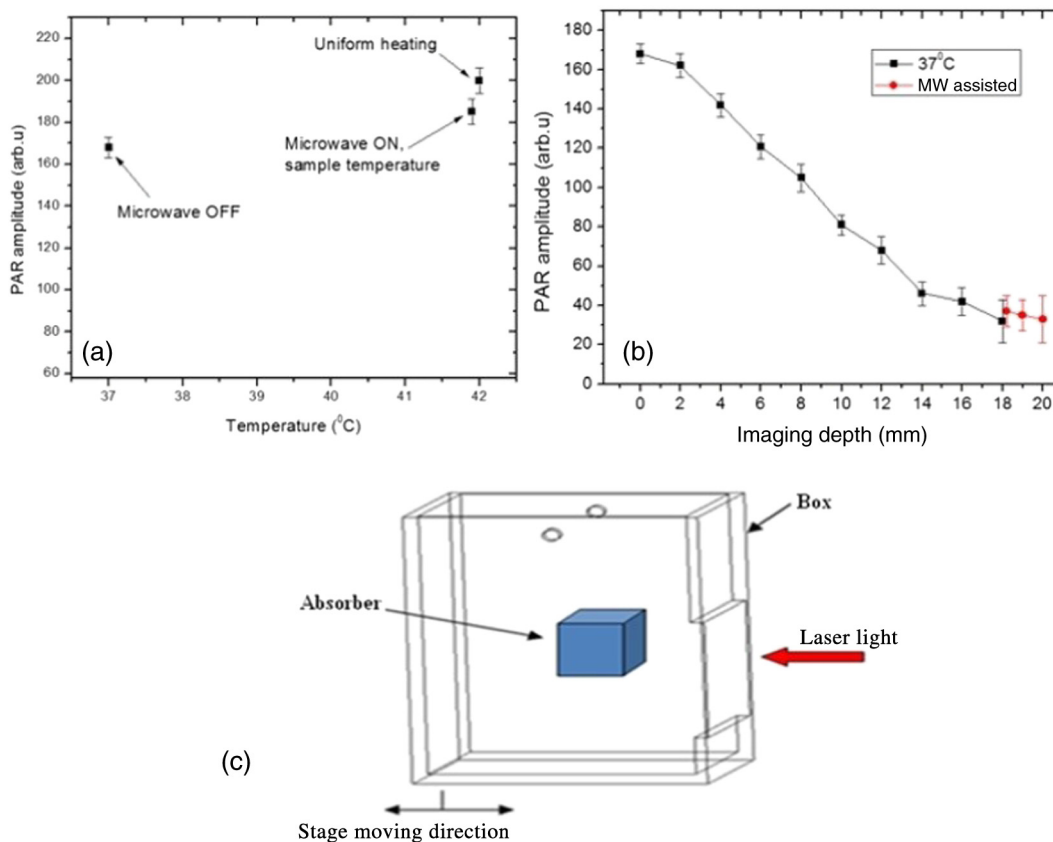
Fig. 4 (a) Measured PAR cross-correlation amplitude peak from *ex vivo* bovine muscle with MW and uniform heating, (b) PAR signal imaging depth study under MW heating, and (c) experimental setup for PAR imaging depth study (the absorber surrounding medium was 0.47% intralipid solution).
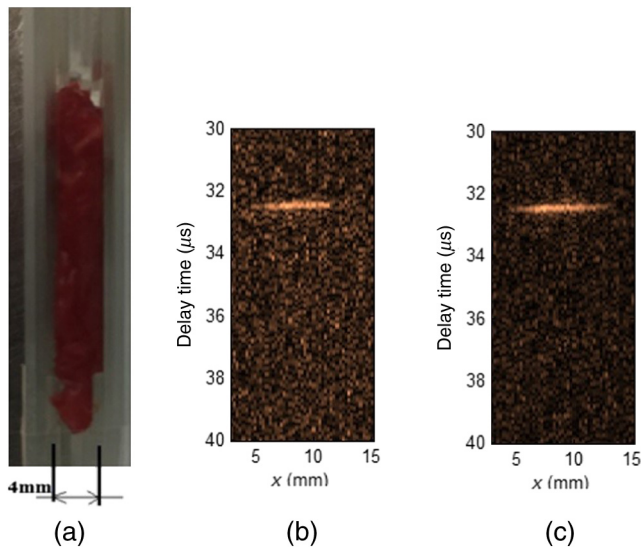
Fig. 5 (a) Picture of a 4-mm wide *ex vivo* bovine muscle sample, (b) one-dimensional image at 37°C with optical scattering, and (c) same imaging conditions as in (b) with added MW heating.

(20%), and the noise was high. With MW heating, the PAR signal became stronger (about 8% increase). The experimental results show that the imaging depth was increased by 11% with MW heating assistance.

Figure 5 shows an experimentally one-line-scanned image of a 4-mm wide *ex vivo* bovine muscle sample. Figure 5(a) is the picture of the sample as it was placed between clamps. Figure 5(b) shows a bright PAR horizontal-line image at ambient temperature 37°C with intralipid solution as the scatterer. The sample was placed 18 mm below the intralipid surface. The scanning signals were collected while moving the laser beam and transducer in tandem across the sample. Figure 5(c) shows the respective image generated with additional MW heating. Comparing Figs. 5(b) and 5(c), the MW-assisted image in Fig. 5(c) appears brighter than in Fig. 5(b) with enhanced contrast against a receding background due to the stronger signal (8% increase).

5 Conclusions

A feasibility investigation of localized MW heating effects on PAR signal enhancement in *ex vivo* bovine muscle was conducted. The localized MW heating was experimentally and theoretically investigated. The calculated and measured results showed agreement at the heated spot over the same heating period and they demonstrated that MW sources can generate a thermal field at low-input-power in bovine muscle for enhancing PAR signals. The PAR SNR increased by about 5% with MW heating assistance for tissue temperature rise up to 42° C, whereas the maximum imaging depth was improved by 11%. MW heating was thus shown to be an effective heating source for biotissues. In view of earlier tissue heating studies,[12] it is concluded that MW heating can be used as a substantially more significant depth resolution enhancement method for PAR imaging of tissues, resulting in up to 13% increase in signal strength and over 20% increase in imaging depth under a localized temperature increase from 37°C to 43°C, provided the MW source can be optimized to generate more uniform subsurface tissue heating around the investigated tissue location than the system developed for this study.

References

1. R. O. Esenaliev et al., "Laser optoacoustic imaging for breast cancer diagnostics: limit of detection and comparison with X-ray and ultrasound imaging," *Proc. SPIE* **2979**, 71–82 (1997).
2. T. Khamapirad et al., "Diagnostic imaging of breast cancer with LOIS: clinical feasibility," *Proc. SPIE* **5697**, 35–44 (2005).
3. X. Wang et al., "Noninvasive laser-induced photoacoustic tomography for structural and functional in vivo imaging of the brain," *Nat. Biotechnol.* **21**, 803–806 (2003).
4. V. G. Andreev, A. A. Oraevsky, and A. A. Karabutov, "Wide-band acoustic pulse detection in opto-acoustic tomography system," in *IEEE Ultrasonics Symp. 2000*, Vol. 2, pp. 1205–1208 (2000).
5. M. Xu and L.V. Wang, "Photoacoustic imaging in biomedicine," *Rev. Sci. Instrum.* **77**, 041101 (2006).
6. W. F. Cheong, S. A. Prahl, and A. J. Welch, "A review of the optical properties of biological tissues," *IEEE J. Quantum Electron.* **26**, 2166–2185 (1990).
7. N. Won et al., "Imaging depths of near-infrared quantum dots in first and second optical windows," *Mol. Imaging* **11**(4), 338–352 (2012).
8. R. Alwi et al., "Silica-coated super paramagnetic iron oxide nanoparticles (SPION) as biocompatible contrast agent in biomedical photoacoustics," *Biomed. Opt. Express* **3**, 2500–2509 (2012).
9. B. Lashkari and A. Mandelis, "Comparison between pulsed laser and frequency-domain photoacoustic modalities: signal-to-noise ratio, contrast, resolution, and maximum depth detectivity," *Rev. Sci. Instrum.* **82**, 094903 (2011).
10. H. I. Robins et al., "A nontoxic system for 41.8 degrees C whole-body hyperthermia: results of a Phase I study using a radiant heat device," *Cancer Res.* **45**(8), 3937–3944 (1985).
11. J. Stang et al., "A preclinical system prototype for focused microwave thermal therapy of the breast," *IEEE Trans. Biomed. Eng.* **59**, 2431–2438 (2012).
12. W. Wang and A. Mandelis, "Thermally enhanced signal strength and SNR improvement of photoacoustic radar module," *Biomed. Opt. Express* **5**, 2785–2790 (2014).
13. W. Wang and A. Mandelis, "Thermally enhanced photoacoustic radar imaging of biotissues," *Int. J. Thermophys.* **36**, 900–904 (2015).
14. G. Kelly, "Body temperature variability (Part 1): a review of the history of body temperature and its variability due to site selection, biological rhythms, fitness, and aging," *Altern. Med. Rev.* **11**(4), 278–293 (2006).
15. P. A. Mackowiak and G. Worden, "Carl Reinhold August Wunderlich and the evolution of clinical thermometry," *Clin. Infect. Dis.* **18**, 458–467 (1994).
16. L. F. Fajardo, "Pathological effects of hyperthermia in normal tissues," *Cancer Res.* **44**(10 Suppl), 4826s–4835s (1984).
17. J. van der Zee, "Heating the patient: a promising approach?," *Ann. Oncol.* **13**(8), 1173–1184 (2002).
18. S. A. Sapareto and W. C. Dewey, "Thermal dose determination in cancer therapy," *Int. J. Radiat. Oncol. Biol. Phys.* **10**, 787–800 (1984).
19. M. R. Horsman and J. Overgaard, "Hyperthermia: a potent enhancer of radiotherapy," *Clin. Oncol.* **19**, 418–426 (2007).
20. P. Sminia et al., "Effect of hyperthermia on the central nervous system: a review," *Int. J. Hyperthermia* **10**, 1–30 (1994).
21. C. L. Brace, "Dual-slot antennas for microwave tissue heating: parametric design analysis and experimental validation," *Med. Phys.* **38**, 4232–4240 (2011).
22. S. Kikuchi et al., "Control of heating pattern for interstitial microwave hyperthermia by a coaxial-dipole antenna-aiming at treatment of brain tumor," *Electron. Commun. Jpn.* **90**, 31–38 (2007).
23. B. Lashkari and A. Mandelis, "Linear frequency modulation photoacoustic radar: optimal bandwidth and signal-to-noise ratio for frequency-domain imaging of turbid media," *J. Acoust. Soc. Am.* **130**, 1313–1324 (2011).

24. P. Keangin, P. Rattanadecho, and T. Wessapan, "An analysis of heat transfer in liver tissue during microwave ablation using single and double slot antenna," *Int. Commun. Heat Mass Transfer* **38**, 757–766 (2011).

25. M. G. Skinner et al., "A theoretical comparison of energy sources-microwave, ultrasound and laser-for interstitial thermal therapy," *Phys. Med. Biol.* **43**, 3535–3547 (1998).

26. W. Chen et al., "Differences in the lesion formation process between focused ultrasound and microwave ablations," *Med. Phys.* **33**, 1346–1351 (2006).

27. V. Frenkel, "Ultrasound mediated delivery of drugs and genes to solid tumors," *Adv. Drug Delivery Rev.* **60**, 1193–1208 (2008).

28. S. A. Telenkov and A. Mandelis, "Fourier-domain biophotoacoustic subsurface depth selective amplitude and phase imaging of turbid phantoms and biological tissue," *J. Biomed. Opt.* **11**, 044006 (2006).

29. V. È Gusev and A. A. Karabutov, *Laser Optoacoustics*, American Institute of Physics, New York (1993).

30. C. E. Cook, *Radar Signals: An Introduction to Theory and Application*, Artech House, Boston, Massachusetts (1993).

31. B. R. Mahafza, *Radar Systems Analysis and Design using MATLAB*, 2nd ed., Chapman & Hall/CRC, Boca Raton, Florida (2005).

32. W. Wang, "Signal strength and SNR enhancement techniques for frequency domain photoacoustic radar imaging," Doctoral Dissertation, Univ. of Toronto (2015).

33. V. A. Dubinskaya et al., "Comparative study of the state of water in various human tissues," *Bull. Exp. Biol. Med.* **144**, 294–297 (2007).

34. N. A. Lange, *Lange's Handbook of Chemistry*, J. A. Dean, Ed., 11th ed., McGraw-Hill, New York (1973).

35. N. Osborne, H. Stimson, and D. Ginnings, "Measurements of heat capacity and heat of vaporization of water in the range 0 degrees to 100 degrees C," *J. Res. Nat. Bur. Stand.* **23**, 197–260 (1939).

36. S. Temkin, *Elements of Acoustics*, John Wiley, New York, Toronto (1981).

37. J. R. Zijp and J. J. ten Bosch, "Optical properties of bovine muscle tissue in vitro; a comparison of methods," *Phys. Med. Biol.* **43**, 3065–3081 (1998).

38. L. M. L. Nollet et al., *Handbook of Meat, Poultry and Seafood Quality*, 1st ed., Blackwell Publishing, Ames, Iowa (2007).

39. R. A. Lawrie, *Lawrie's Meat Science*, 7th ed., CRC Press, Boca Raton, Florida (2006).

40. A. M. Pearson and R. B. Young, *Muscle and Meat Biochemistry*, Academic Press, San Diego, California (1989).

41. Y. Choi and M. R. Okos, "Effects of temperature and composition on the thermal properties of foods," in *Food Engineering and Process Applications: Transport Phenomena*, M. L. Maguer and P. Jelen, Eds., Vol. **1**, pp. 93–101, Elsevier Applied Science, Amsterdam, The Netherlands (1986).

42. S. M. Nikitin, T. D. Khokhlova, and I. M. Pelivanov, "Temperature dependence of the optoacoustic transformation efficiency in ex vivo tissues for application in monitoring thermal therapies," *J. Biomed. Opt.* **17**, 061214 (2012).

43. J. Shah et al., "Photoacoustic imaging and temperature measurement for photothermal cancer therapy," *J. Biomed. Opt.* **13**(3), 034024 (2008).

44. M. Pramanik and L. V. Wang, "Thermoacoustic and photoacoustic sensing of temperature," *J. Biomed. Opt.* **14**, 054024 (2009).

45. D. Hardie, A. Sangster, and N. Cronin, "Coupled field analysis of heat flow in the near field of a microwave applicator for tumor ablation," *Electromagn. Biol. Med.* **25**, 29–43 (2006).

46. F. A. Duck, *Physical Properties of Tissue: A Comprehensive Reference Book*, Academic Press, London (1990).

47. H. Pennes, "Analysis of tissue and arterial blood temperatures in the resting human forearm," *J. Appl. Physiol.* **1**(2), 93–122 (1948).

48. W. L. Nyborg, "Solutions of the bio-heat transfer equation," *Phys. Med. Biol.* **33**, 785–792 (1988).

49. A. Mandelis and J. Vanniasinkam, "Theory of nonradiative decay dynamics in intensely pumped solid-state laser media via laser photothermal diagnostics," *J. Appl. Phys.* **80**, 6107–19 (1996).

50. K. D. Cole et al., *Heat Conduction using Green's Functions*, 2nd ed., CRC Press, Boca Raton (2011).

51. I. Kiricuta and V. Simplaceanu, "Tissue water-content and nuclear magnetic-resonance in normal and tumor tissues," *Cancer Res.* **35**(5), 1164–1167 (1975).

52. C. Gabriel, S. Gabriel, and E. Corthout, "The dielectric properties of biological tissues: I. Literature survey," *Phys. Med. Biol.* **41**, 2231–2249 (1996).

53. S. Gabriel, R.W. Lau, and C. Gabriel, "The dielectric properties of biological tissues. II. Measurements in the frequency range 10 Hz to 20 GHz," *Phys. Med. Biol.* **41**, 2251–2269 (1996).

54. S. Gabriel, R. W. Lau, and C. Gabriel, "The dielectric properties of biological tissues. III. Parametric models for the dielectric spectrum of tissues," *Phys. Med. Biol.* **41**, 2271–2293 (1996).

55. W. T. Joines et al., "Microwave power absorption differences between normal and malignant tissue," *Int. J. Radiat. Oncol. Biol. Phys.* **6**, 681–687 (1980).

56. M. Lazebnik et al., "A large-scale study of the ultrawideband microwave dielectric properties of normal, benign and malignant breast tissues obtained from cancer surgeries," *Phys. Med. Biol.* **52**, 6093–6115 (2007).

57. R. Pethig, "Dielectric properties of body tissues," *Clin. Phy. Physiol. Meas.* **8**(Suppl A), 5–12 (1986).

58. H. J. van Staveren et al., "Light scattering in Intralipid-10% in the wavelength range of 400–1100 nm," *Appl. Opt.* **30**, 4507–4514 (1991).

Wei Wang received his bachelor's degree at Xi'an Polytechnic University, China, his master's degree from the University of Western Ontario, and his PhD from the University of Toronto. His research interests are PA imaging, optical imaging, ultrasound imaging, and thermal imaging.

Andreas Mandelis is a full professor of mechanical and industrial engineering and electrical and computer engineering at the Institute of Biomaterials and Biomedical Engineering, University of Toronto. He is the director of the Center for Advanced Diffusion-Wave and Photoacoustic Technologies (CADIPT), University of Toronto. His research interests include instrumentation and measurement science, nondestructive and noninvasive imaging and sensors, PA, photothermal and diffusion-wave physics and imaging technologies, signal processing, biothermophotonic laser diagnostics, nondestructive testing and imaging, and semiconductor optoelectronics.